Journal of Nuclear Materials 397 (2010) 8–18

Contents lists available at ScienceDirect

Journal of Nuclear Materials

journal homepage: www.elsevier.com/locate/jnucmat

Impact of auto-irradiation on the thermophysical properties of oxide nuclear reactor fuels

D. Staicu *, T. Wiss, V.V. Rondinella, J.P. Hiernaut, R.J.M. Konings, C. Ronchi

European Commission, Joint Research Centre, Institute for Transuranium Elements, 76125 Karlsruhe, Germany

ARTICLE INFO

Article history:
Received 5 December 2008
Accepted 26 November 2009

ABSTRACT

The effect of α-damage on the thermophysical properties of UO_2 was investigated using samples doped with ^{238}Pu. Characterisations were performed after different storage periods, including X-ray diffraction to monitor the lattice parameter evolution, Knudsen-cell helium release experiments and transmission electron microscopy examinations. The apparent heat capacity was measured by differential scanning calorimetry and the recovery stages observed were attributed to the recombination of a certain kind of point or extended defect. The thermal diffusivity, measured by the laser-flash technique during annealing cycles, displayed similar recovery stages. The measurements show that the degradation of the diffusivity with increasing α-dose is not linear, and that saturation occurs at relatively low doses. A correlation quantifying this degradation is proposed. Comparison with the thermal diffusivity of very low burn-up rector irradiated samples, where the main source of degradation is radiation damage, shows that the annealing stages are similar.

1. Introduction

Nuclear fuel assemblies are used in the reactor for 3–6 years, and are subsequently stored in an on-site pool at relatively low temperature. During this cooling phase, radioactive decay damage and helium begin to accumulate in spent fuel. Samples of spent fuel are normally extracted for post-irradiation examination after a few years of cooling, when the radioactivity level has sufficiently decreased. In order to assess the in-pile value of thermophysical properties using out-of-pile measurements, the effect of decay damage has to be distinguished from that caused by fission during reactor operation. This makes the interpretation of the experiments difficult, and specific methods and verifications have to be applied.

At the Institute for Transuranium Elements (ITU) a study was initiated aimed at understanding the radiation effects on the thermophysical properties of oxide nuclear fuels. The project has the twofold objective of studying the effect of burn-up on the thermal performance of operating fuel, and of providing information on the evolution of spent fuel under repository conditions. Previous studies had been conducted on reactor irradiated fuels in which lattice damage from fission and decay coexist [1]. The work being mainly focused on decay damage, the investigation is carried out on samples where the lattice defects are created by α-decay. If an α-emitter is homogeneously distributed in the fuel matrix, the damage produced is well defined in dose and nature. This damage is characterised by two simultaneous processes: that due to the highly energetic alpha particles, which create ionisation and, at the end of the range a few hundreds of atomic displacements, and that due to the heavy, less energetic recoil atoms which produce thousands of atomic displacements. The individual volumes affected by the two types of damage are well separated by thousands of unit cell distances. Furthermore, α-helium is also formed in smaller concentrations than point defects and, being frozen in the lattice, provides an additional possibility to investigate the interaction of gas-in-solid with lattice defects.

The goal of the present study is to obtain a consistent description of the radiation damage nature and of its effects on the thermal conductivity of the α-doped samples. Even if these samples represent a simplified system as compared to reactor irradiated fuel, the combination of characterisation results obtained with different techniques is required. Transmission electron microscopy (TEM) and scanning electron microscopy (SEM) are used for the observation of dislocation loops and bubbles. The concentration of point defects is investigated by measuring the evolution of the lattice parameter and the heat released during the annealing of damaged samples. Finally, these observations are correlated with thermal conductivity measurements. For comparison purposes, the effect of in-pile radiation damage is also considered by studying low burn-up reactor irradiated fuel.

2. Samples

The α-doped samples were chosen for the main part of this study because they represent a simplified system as compared to

* Corresponding author. Tel.: +49 7247 951263; fax: +49 7247 95199628.
E-mail address: dragos.staicu@ec.europa.eu (D. Staicu).

0022-3115/$ - see front matter © 2009 Elsevier B.V. All rights reserved.
doi:10.1016/j.jnucmat.2009.11.024

reactor irradiated fuel, and a significant amount of irradiation dose can be accumulated in relatively short periods of time. Such samples are compatible with the experimental techniques installed in non-shielded glove-boxes, allowing a broad range of characterisations to be applied. The damage source, storage time and temperature can be defined with precision. As compared to standard reactor irradiated fuel, the interpretation of the results is simpler. For this reason, the reactor irradiated fuel considered in this study has very low burn-up and was irradiated under special conditions.

2.1. Alpha doped samples

The α-doped samples were produced by incorporating 0.1 (sample UO_2-01) and 10 wt.% (sample UO_2-10) of an additive containing 66.7 wt.% $^{238}PuO_2$ (half-life of 87 years) in natural UO_2 by a sol–gel process [2]. The other components of the additive are: 21.1 wt.% of other Pu isotopes, 12.1 wt.% of ^{234}U and 0.1 wt.% of ^{241}Am. A homogeneous solid solution was obtained with a density of 94% of the theoretical value.

An estimation of the upper limit for the concentration of point defects created by auto-irradiation can be directly obtained if the recombination processes are neglected. For instance, the α-decay dose accumulated in the UO_2-10 sample during 6 months is 5.6×10^{18} cm^{-3}, with a corresponding energy deposition rate of about 0.1 W cm^{-3}. Each α-particle (energy of 5.499 MeV) creates about 66 U displacements (displacement energy threshold 40 eV) and 140 O displacements (displacement energy threshold 20 eV), whilst the ^{234}U recoil atom (energy of 92 keV) creates 295 U and 1180 O displacements (TRIM code predictions [3]). If damage overlapping and recombination are not considered, the total defect concentrations are 2.0×10^{21} cm^{-3} for uranium and 7.3×10^{21} cm^{-3} for oxygen Frenkel pairs. As the atomic density of UO_2 is 7.0×10^{22} atoms cm^{-3}, the displacements per atom (dpa) value is of the order of magnitude of 0.1. In fact only a small fraction of defects created is effectively present as point defects at these damage doses. The majority either recombine or interact with other defects to form less energetic extended configurations, and it is the objective of the present work to quantify these phenomena and their effect on the thermal conductivity.

2.2. VOLEX samples (reactor irradiated)

Polycrystalline UO_2 samples were irradiated in the HFR, Petten (VOLEX experiment) under effectively uniform and constant temperature. These conditions were achieved by placing the samples in stainless steel capsules. The original goal of the experiment was to study the swelling due to point defects at very low burn-ups. The sample selected for this study was irradiated up to a dose of 10×10^{18} fissions cm^{-3}, corresponding to a burn-up of about 0.4 MWd/t. The irradiation lasted 19 days and the sample was kept under a uniform temperature of 570 K. In this sample, the in-pile produced damage is the main source of thermal diffusivity degradation, because the concentration of fission products is small. The irradiation took place in 1988 and the experiments were performed in 2003.

3. Experimental procedure

This section presents the experimental methodology that was applied and some fundamental results that are important for this study. For the α-doped samples, different experiments were conducted according to a long time schedule starting from a sample reference state ($t = 0$) at the end of 1997. In 1998, some specimens in the form of powder were annealed and prepared for X-ray diffraction (XRD), and thereafter the lattice parameter was measured at established time intervals. Knudsen-cell helium release experiments and TEM examinations were started after 4 years. After approximately 5 years the degradation and recovery of the thermal diffusivity of the samples was measured during thermal annealing programs. Then, after further 6 months, the specific heat was measured, and the experiment was repeated two times, respectively at 6 and 5 months intervals. For comparison purposes, thermal diffusivity measurements were also performed for the VOLEX samples.

3.1. XRD: lattice parameter as indicator of radiation damage and recovery

The XRD technique is used in this study to measure the lattice parameter as a function of the storage time. However, the relation between the value of the lattice parameter and the concentration of defects is still a matter of investigation. A reference can be taken from the known variation of the lattice parameter in non-stoichiometric (U, Pu)O_2, from which a first estimate of the magnitude of the oxygen vacancy concentration can be obtained. The lattice parameter is 5.4706×10^{-1} nm for UO_2 [4], and 5.39580×10^{-1} nm for PuO_2 [5]. The lattice parameter of (U, Pu)O_2 can be predicted by using Vegard's law. As a correlation for the variation of the lattice parameter as a function of the oxygen Frenkel pairs concentration is not available, a reasonable approach can be based on the lattice parameter variation in hypostoichiometric low Pu-content (U, Pu)O_2 and in hyperstoichiometric UO_2. According to Duriez et al. [6] and Ohmichi et al. [4] the increase rate of the lattice parameter of (U, Pu)O_{2-x} as a function of stoichiometry deviation (oxygen vacancies) is $da/d(O/M) = 32 \times 10^{-3}$ nm. This dilatation in the presence of oxygen vacancies is described by Eq. (1):

$$a = 0.54706 + 0.032x \text{ nm} \quad (1)$$

For UO_2, literature data [7] indicate a lattice contraction in the presence of extra oxygen and consequent formation of U^{+5} ions:

$$a = 0.54706 - 0.01306x \text{ nm} \quad (2)$$

Combining these two correlations, for stoichiometric fuel containing y oxygen Frenkel pairs one obtains:

$$a = 0.54706 + 0.019y \quad \text{and } \Delta a = 0.019y \text{ nm} \quad (3)$$

This correlation gives the lattice parameter change linked to a given concentration of oxygen Frenkel pairs, while the measured lattice parameter change integrates also the effect of other damage. The main results of a bibliographic study, done in order to clarify this aspect, are now presented.

The lattice parameter variation was measured by Weber [8] during isochronal (30 min) and isothermal annealing for UO_2 *single crystals* irradiated by with α-particles emitted from a $^{238}PuO_2$ source, up to 0.06 dpa. Three annealing stages appeared at, respectively, ~570 K, ~850 K and ~1200 K; complete annealing was found at ~1300 K. It was found that the recovery for the first stage is slow and gradual at 570 K and becomes much faster at 670 K. For the two last stages, recovery is always very fast once the characteristic temperature is reached. This suggests that the kinetic controlling processes are single-energy thermally activated. The distinct stages are resulting from migration and annealing of different lattice defect species by recombination, clustering or annihilation at sinks. Weber [9] showed that the amplitude of the three recovery stages was almost equal:

- stage I was attributed to the migration and recombination of oxygen interstitials (activation energy of about 1.5 eV);
- stage II was attributed to the migration and recombination of uranium vacancies (activation energy of about 2.2 eV); and
- stage III was attributed to α-helium trapped in vacancies and released via dissociation from vacancy–helium complexes.

Concerning the last stage, Cavaleru et al. [10] also observed in constant heating-rate experiments that the major gas release peak in helium-implanted UO_2 single crystals occurred at ~1250 K, with an activation energy of 3–4 eV.

Similarly, geologically self-irradiated single crystals of uraninite and thorianite (U, Th)O_2 (up to doses of 130–170 dpa) were annealed and the lattice parameter was measured by Evron et al. [11]. Again three recovery steps were observed at about 470 K, 870 K and 1200 K. Annealing up to 1470 K showed no further evolution. The fractional recovery, for single crystals, was found to be very similar for α-damage, recoil damage and fission damage. The interpretation of the three recovery stages was similar to the one proposed by Weber [9]. For the third stage, the relevant gases are helium from α-particle bombardment or from internal α decay, and krypton and xenon from fission.

Nakae et al. [12] measured the increase of the lattice parameter of reactor-irradiated samples, as a function of the fission dose for polycrystalline UO_2 (with two grain sizes) and observed three successive stages. Then the samples were annealed up to 780 K, and two recovery stages were observed at, respectively, 470 K and 600 K (whereby only the first one was clearly detected at low doses). The normalised lattice parameter recovery stages observed in α-irradiated UO_2 single crystals were found to correspond very well to the normalised recovery stages observed in fission-damaged UO_2 single crystals [9]. These results show that the recovery of the lattice expansion occurs by similar mechanisms in α- and fission-damaged UO_2.

3.2. Thermal conductivity degradation and recovery during annealing

The laser-flash technique [13] is used in this work to investigate the effect of radiation damage on the thermal diffusivity and thermal conductivity of the fuel. Thermal annealing cycles with increasing maximum temperatures were used in order to investigate the temperature dependence of the radiation damage recovery. The thermal conductivity in UO_2 is dominated by the phonon heat transport mechanism that is typically described, at moderate to high temperatures, by the simple relation [14]:

$$\lambda_{phonon} = \frac{1}{A + BT} \tag{4}$$

The temperature dependent term is referred as the *Umklapp* process, resulting in a linear relationship with T of the thermal resistivity. The A coefficient is linked to the concentration of phonon scattering centres. Among radiation effects, lattice point defects, or any substitutional or accommodated foreign atom which displaces U/Pu or O out of their normal lattice positions constitutes a scattering centre of phonons. Linear defects, such as dislocations, act as much less effective scattering centres because they impose much weaker local strain to the lattice. Larger agglomerates such as porosity, bubbles, and solid precipitates have the least phonon scattering efficiency.

During the annealing cycles of the thermal diffusivity, a temperature is reached at which the isolated point defects are able to diffuse to form precipitates or bubbles and thus decreasing the number of phonon scattering centres. Therefore, during the complete annealing cycle, a sequence of recovery stages is found.

As for the lattice parameter, a correlation between the concentration of defects and the thermal conductivity degradation is not available and results obtained for non-stoichiometric (U, Pu)O_2 are used. As for the lattice parameter evolution, the effect of oxygen defects on the thermal conductivity is evaluated from the effect of non-stoichiometry. For hypostoichiometric and low Pu-content mixed oxide (3–15% Pu), Duriez et al. [6] found:

$$A(x) = 2.85x + 0.035 \text{ mK W}^{-1} \tag{5}$$

A similar formula was proposed by Carbajo [15]: $A(x) = 3.336x + 0.0257$ mK W^{-1}. For the hyperstoichiometric oxide, Amaya [7] found an equivalent increase of $A(x)$, showing that the effect on the thermal conductivity is effectively the same for oxygen vacancies and interstitials.

The effect of the accumulation of radiation damage on the thermal conductivity was investigated by Schmidt et al. [16] for PuO_2, AmO_2 and Am_2O_3. The relative conductivity change as a function of the α-decays per cm^3, n_α, was found to follow an exponential growth equation of the form:

$$\Delta\lambda/\lambda = H(1 - \exp(y/n_\alpha)) \tag{6}$$

the growth rate y being the same for the three materials investigated ($y = 5.88 \times 10^{-18}$). The amplitude of the maximum decrease (H) reflects the saturation effect and depends on the kind of material.

3.3. Apparent specific heat measured by DSC

The apparent specific heat, C_p^*, of damaged samples was measured by differential scanning calorimetry (DSC) by applying ascending and descending temperature programmes in the range 400–1500 K. The real $C_p(T)$ obtained from literature data for (U, Pu)O_2 corresponds to the average between the ascending and descending curves of "fresh", undamaged samples. Calorimetry of strong α-emitters is perturbed by the heat generated by radioactive decay. In fact, the apparent temperature-ascending curve of C_p^* is lower than the real C_p, whilst the descending curve is higher. However, the average of these two curves gives exactly the value of the unbiased C_p. The α-decay heat generated by the sample is known to be 0.76 W cm^{-3} for the UO_2-10 sample with 5.499 MeV energy per α-particle and the same energy for the recoil daughter. Knowing this energy source, whose effects are perfectly anti-symmetric in the ascending and descending curves, the calorimetric signal could be accurately calibrated in terms of energy, for a given heating rate.

For radiation damaged samples, the deviation of the measured $C_p^*(T)$ from the real heat capacity, $C_p(T)$, is also related to the recovery of the latent heat of the lattice defects during thermal healing. After calibration, this released energy can be accurately measured. Finally, if the energy release associated to the recovery of a single defect is known, the concentration of defects can be deduced. An advantage of this technique is that the heat released is proportional to the defects concentration, no saturation effects can take place. Another advantage is that the experiment is done at constant heating rate and is continuous, allowing a precise assessment of the temperature range where recombinations take place.

4. Results for the alpha doped samples

4.1. XRD results

The lattice parameter of the α-doped samples increases as a function of time, and, though the slope of the curve decreases with time, no saturation was reached after 4 years of storage (Fig. 1). Therefore, if 1/3 of the variation of the lattice parameter in the UO_2-10 sample during the 6 months of dose accumulation is due to oxygen defects only [9], the corresponding concentration of oxygen Frenkel pairs producing the same effect is of $x = 0.014$ (Eq. (1)). Furthermore, the contribution of the defects in the cation sub-lattice (U and Pu) to the increase of the lattice parameter being almost equal to that of oxygen defects [9], the concentration of these defects can be considered to be of the same order of magnitude as that of the oxygen defects. If this assumption is maintained, the concentration of oxygen and uranium vacancies in the sample is 3×10^{20} cm^{-3}.

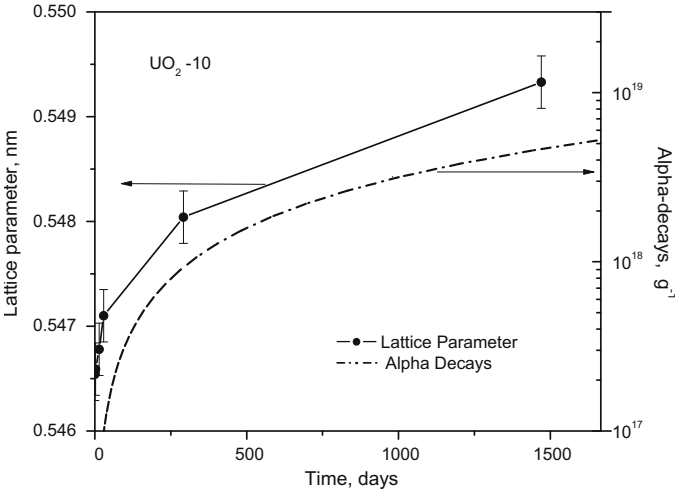

Fig. 1. Lattice parameter of the α-doped (UO_2-10) [20].

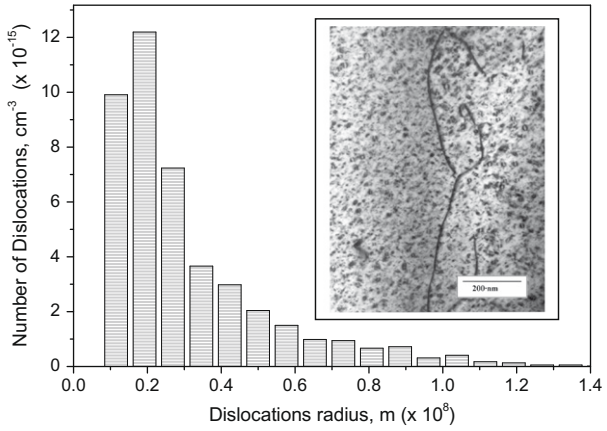

Fig. 2. TEM micrograph showing the dislocation loops with size histogram for the UO_2-10 sample.

4.2. TEM observations and Knudsen-cell helium release experiments

TEM examinations (Fig. 2) and Knudsen-cell mass spectrometric helium release experiments were carried out on the UO_2-10 sample at $t = 4$ years. The dislocation loops size distribution was measured by manual image analysis from the starting configuration after damage accumulation (Fig. 2) through the various annealing stages. The dislocation loops being an extended defect formed by precipitation of point defects, the number of point defects involved could be determined form the size distribution (cf. Section 5). Though very small loops can be seen to be formed at room temperature, they fully developed only at temperatures between 1100 K and 1200 K, temperatures at which the black dots (un-relaxed defect clusters) disappear. A major helium release is observed at about 1200 K (Fig. 3) during the Knudsen-cell measurement. This temperature is in agreement with literature data [8,11].

4.3. Measurement of thermal diffusivity during annealing

The thermal diffusivity was measured in samples UO_2-01 and UO_2-10 after a storage time of approximately 5 years. The diffusivity was normalised to 5% porosity. The results (Fig. 4) show that the thermal diffusivity of UO_2-10 is lower that the one of UO_2-01, both before and after annealing. This effect is due to the difference in Pu content and in α-dose. The number of annealing cycles was of 11

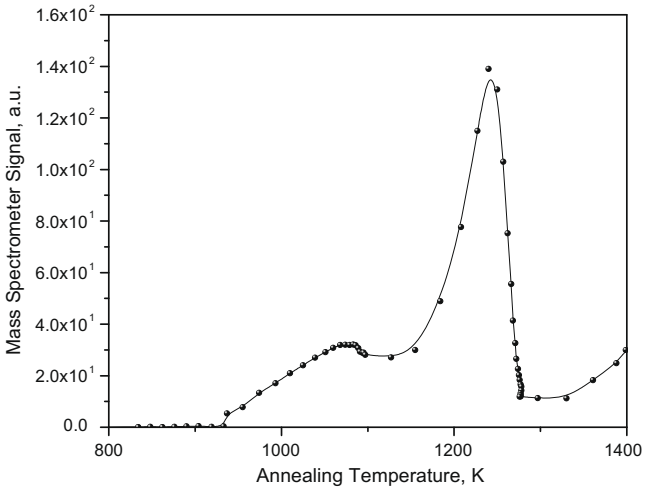

Fig. 3. The Knudsen-cell He release for UO_2-10. The resulting enthalpy of diffusion deduced from the analysis of the major peak [21] is 190 kJ mol^{-1} (2 eV). This is in agreement with the value obtained in the calorimetry measurements.

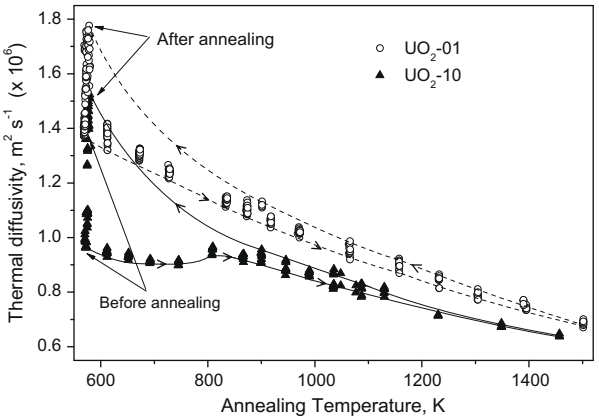

Fig. 4. Thermal diffusivity of samples UO_2-01 and UO_2-10 (corrected to 5% porosity). The lines show the envelope curves before and after annealing, the intermediary annealing cycles are not shown.

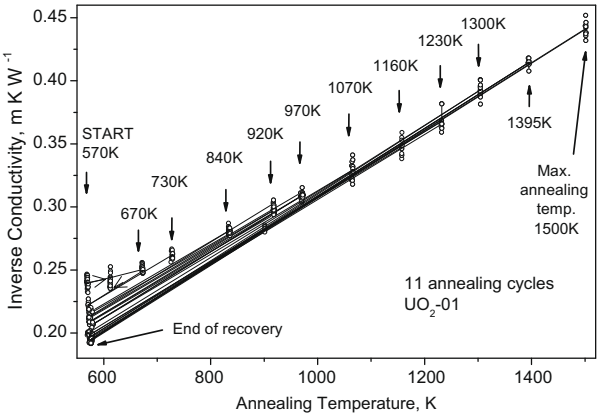

Fig. 5. Inverse thermal conductivity of the sample UO_2-01 measured during 11 annealing cycles with increasing maximum temperature.

for UO_2-01 and of 15 for UO_2-10. The inverse conductivity values obtained after each annealing cycle are plotted in Figs. 5 and 6 and are linearly dependent on temperature in agreement with

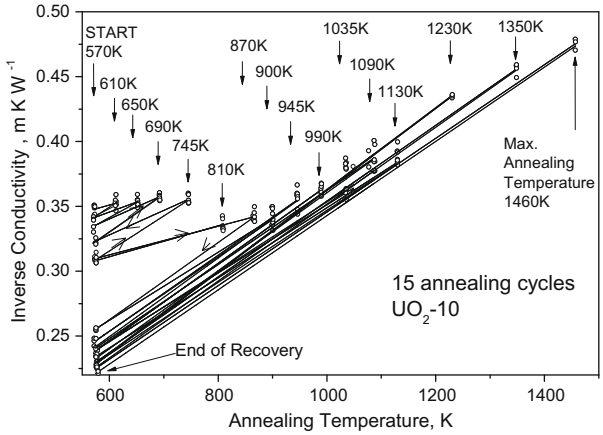

Fig. 6. Inverse thermal conductivity of sample UO_2-10 measured during 15 annealing cycles with increasing maximum temperature.

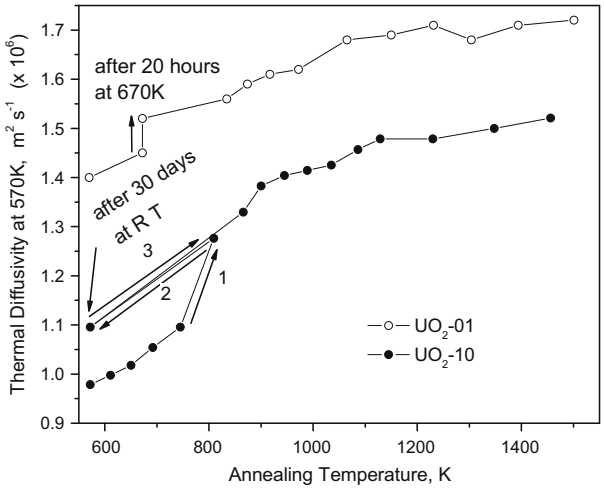

Fig. 7. Diffusivity at 570 K as a function of the maximal annealing temperature in the (U, Pu)O_2 samples. The sample UO_2-01 was kept at 670 K during 20 h. After an annealing at 810 K, the sample UO_2-10 was kept at ambient temperature during 30 days, then the thermal diffusivity was measured again at 570 K and the annealing studies continued at higher temperatures (sequences 1-2-3).

Eq. (4). The values obtained during ascending temperature measurements are not considered in this plot because recovery of damage takes place during heating. Under these conditions the inverse conductivity is not linearly dependent on temperature but this does not constitute a contradiction with Eq. (4) because it is not applicable as concentration of radiation damage changes during this process. The recovery effects were measured by the diffusivity changes at the lowest measurement temperature (570 K), at which the effect of radiation damage has the highest magnitude. The diffusivity at 570 K as a function of the maximal annealing temperature is plotted in Fig. 7. In order to examine the time dependence of recovery at constant temperature and the rate at which defects are re-created, two special measurements were performed (Fig. 7):

- The sample UO_2-01 was kept at 670 K during 20 h and the diffusivity was measured as a function of time. A moderate increase was observed.
- After an annealing at 810 K, the sample UO_2-10 was kept at ambient temperature during 30 days, and then the thermal diffusivity was measured again at 570 K. A relatively strong decrease was observed (Fig. 7): the decease was about the half of the one observed for a storage time of 5 years.

Measurements of the diffusivity variation during isothermal annealing were also performed at higher temperatures; however no significant effect was observed since during the temperature stabilisation of the furnace (30–40 min) isochronal annealing conditions could not be precisely maintained. Therefore, the recovery effects were better deduced from the hysteretic effects at low temperature. The thermal conductivity, interpolated by the $1/(A + BT)$ law, gives the values of A and B coefficients as plotted in Figs. 8 and 9. Taking into account the position of the annealing steps observed during the DSC measurement discussed in the next section, the results can be interpreted as follows:

- Sample UO_2-01: a first annealing at ~670 K, a second between 850 K and 950 K, and a third between 1250 K and 1300 K.
- Sample UO_2-10: a first annealing between 600 and 700 K, a second between 850 K and 1000 K, and the third between 1150 K and 1250 K.

Ignoring at this step the saturation effect, these results can be used to obtain an estimate of the magnitude of the concentration of oxygen defects. For UO_2-10, the experiment was repeated for a storage time of 6 months and the variation of A during the first annealing step was of 0.12 mK W^{-1}, corresponding to $x = 0.02$ if Eq. (5) is applied. No significant difference is observed between samples stored 5 years and 6 months. This leads to an estimate of the defect concentration of 4×10^{20} cm^{-3} oxygen Frenkel pairs, that is in reasonable agreement with the value deduced from the analysis of the XRD measurements.

After storing the sample at room temperature for 30 days, about 70% of the A value recovered during the previous annealing steps was re-established by the α-radiation. This shows that the effect of the oxygen defect concentration on the thermal conductivity saturates much more rapidly than in the case of the lattice parameter. As for the effect of uranium defects, their effect seems to further increase with the dose (see the comparison of the second stages of the plots of Figs. 8 and 9). The higher proportion of defects annealed at about 800 K in sample UO_2-10 is consistent with its higher α activity.

In order to obtain a correlation linking the alpha dose to the thermal conductivity degradation for UO_2 and low Pu content (U, Pu)O_2, the results obtained for the α-doped samples, and other results obtained on (U, Pu)O_2 fuels were considered (Fig. 10). Adopting Eq. (6) for the interpretation, the best agreement with the experimental results was found with the same growth rate as measured by Schmidt ($y = 5.88 \times 10^{-18}$) and the degradation of the thermal conductivity can be approximated by:

$$\Delta\lambda/\lambda = 0.38(1 - \exp(y/n_\alpha)) \tag{7}$$

The same dependence can be proposed for the A and B coefficients (Fig. 11):

$$\Delta A = 0.22(1 - \exp(y/n_\alpha))\ \text{mK W}^{-1} \tag{8}$$

$$\Delta B = -2.1 \times 10^{-4}(1 - \exp(y/n_\alpha))\ \text{mW}^{-1} \tag{9}$$

4.4. Apparent specific heat of α-doped samples

Three successive DSC measurement campaigns were performed, at time intervals of about 6 months.

During the first campaign C_p^* measurements were carried out with temperature increasing linearly (40 K min^{-1}) between 450 K and 1450 K with a plateau (10 min) at 840 K, intended to complete the first recovery stage. This procedure was used in order to separate the heat effects associated to the annealing of the different kinds of defects. For UO_2-10 the exothermic effect due to damage healing began between 650 K and 700 K and ended at about

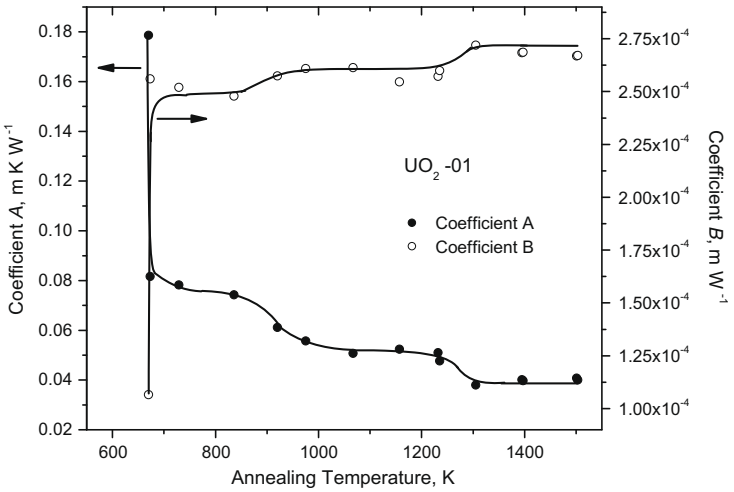

Fig. 8. *A* and *B* coefficients for the sample UO_2-01. The lines are drawn with the assumption of three main annealing steps having characteristic temperatures in the same range as determined by DSC.

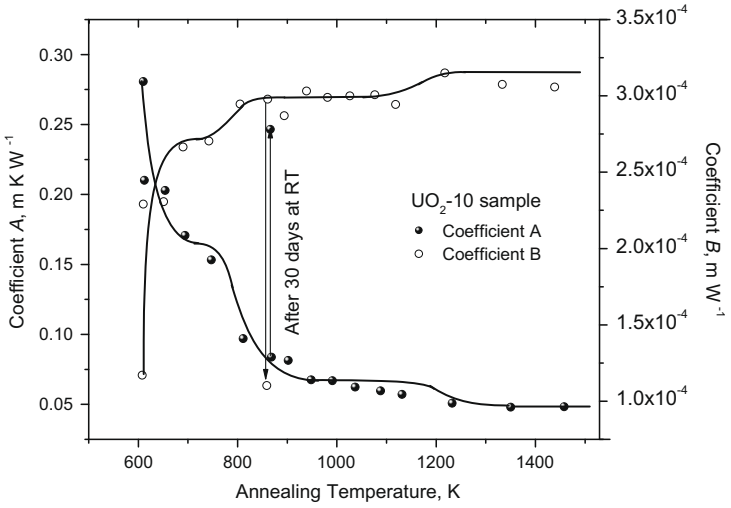

Fig. 9. *A* and *B* coefficients for the highly radioactive sample UO_2-10. The lines are drawn with the assumption of three main annealing steps having characteristic temperatures in the same range as determined by DSC.

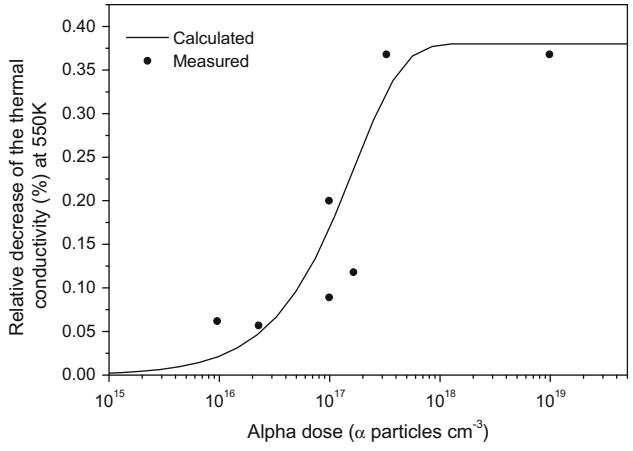

Fig. 10. Relative thermal conductivity decrease as a function of the α-dose for UO_2 and (U, Pu)O_2 samples. The calculated curve was obtained using Eq. (4).

1150 K. Under the chosen thermal annealing conditions the intensity of this effect was very high, the apparent C_p^* being up to 50% lower than C_p, and the total released energy of about 40 J g^{-1}. An exothermic effect was also observed for the sample UO_2-01, in which the damage rate was two orders of magnitude lower; its intensity was, however, very weak (about 4 J g^{-1}). It began at about 650 K, reached a maximum at about 800 K and ended at about 850 K.

A second experiment was performed 6 months after the first one, and, for confirmation purposes, a third one followed after further 5 months (Fig. 12). In both campaigns the heating rate was reduced to 15 K min^{-1} and no temperature plateau was applied. The results of these two campaigns are very similar. The peaks of the latent heat effects appear at temperatures corresponding to the damage healing stages reported above. However, the peak temperatures of the different annealing stages are obviously dependent on the thermal annealing rate, since the controlling mechanisms are very likely single-energy activated processes. Thus the C_p^* peaks appear at slightly higher temperatures on the curve in Fig. 12 if compared with the corresponding values charac-

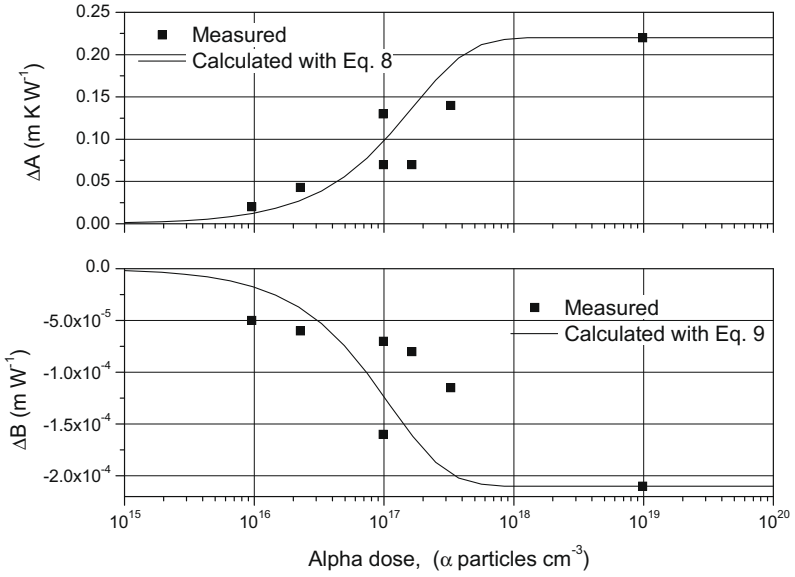

Fig. 11. Variation of the *A* and *B* coefficients as a function of the α-dose for UO_2 and (U, Pu)O_2 samples.

terising the recovery stages in the thermal diffusivity measurements (Fig. 9). This is due to the higher heating rate during the calorimetric measurement (15 K min^{-1} *vs.* 0.5 K min^{-1}). No measurable heat effect was observed for the sample of UO_2-01 during the two last measurement campaigns.

5. Interpretation

5.1. Kinetics of radiation-damage healing

The $C_p^*(T)$ curve can be converted into energy release and analysed in order to identify the different parameters of the latent heat effects. For each stage, the quantities to be derived are concentration and energy associated to the annealing of each kind of defect, as well as its characteristic mobility (*i.e.*, pre-exponential factor and activation energy of the diffusion coefficient). The first step of the analysis of the measured $C_p^*(T)$, aimed at identifying the different stages of the damage annealing, is the separation of the effective peaks. Whilst their respective areas, proportional to the total latent energy release in the individual stages, are independent of the annealing rate, the peaks are displaced towards higher temperatures as this rate increases. The positions of each peak can be used to deduce the apparent diffusion coefficient parameters of the defect involved in the individual stages. Once the peaks are separated, the energy released in the various stages can be evaluated from the respective areas, and, if the defect concentration is known, their formation enthalpy can be eventually deduced.

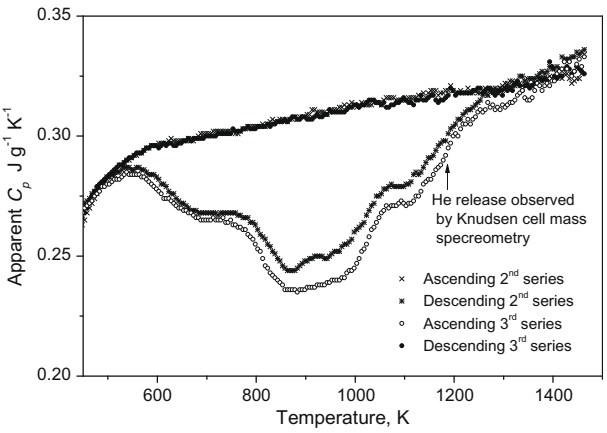

Fig. 12. Apparent C_p^* obtained by DSC respectively during the first and second runs for UO_2-10.

The main defects to consider when interpreting the thermal annealing stages are oxygen and uranium vacancies and interstitials in the respective sub-lattices and helium complexes. Defect/impurity interactions and different defect configurations must also be considered [17]. The Reaction-rate formalism [18] can be used to calculate the evolution of defect concentration in an irradiated material in the presence of void formation and development of dislocation loops. As a starting condition, it is assumed that the material contains a concentration of void embryos and a volume concentration of interstitial loops. Each of these species grows in size because of a net flow of irradiation-produced interstitials to the dislocation loops. The interstitial and vacancy concentrations, c_i and c_v, are determined by the equation system:

$$\begin{aligned} K - D_i c_i k_i^2 - \alpha c_i c_v &= \frac{dc_i}{dt} \\ K' - D_v c_v k_v^2 - \alpha c_i c_v &= \frac{dc_v}{dt} \end{aligned} \tag{10}$$

where K is the displacement damage rate (in dpa/s) and $K' = K + K_e$ (K_e is the rate of thermal vacancy emission from all sinks in the matrix), α is the recombination coefficient. The linear terms represent the point defect losses (k_i and k_v characterise the net capture rates) to the effective sinks (voids, dislocations, grain boundaries, etc.), and the quadratic terms represent the losses due to mutual recombination. D_i and D_v are the respective diffusion coefficients of vacancy and interstitial.

The physical meaning of the equation parameters is self evident, but their magnitude is difficult to predict or to measure. Furthermore, in order to calibrate this model, the initial concentration of interstitials and vacancies, as well as the sink strengths are to be determined. In order to perform this calculation, a simple model for defect annealing is required, relating defect mobility to calorimetric effects. We assumed for this purpose that annealing of each kind of defect is a single-energy activated process and the reaction (recombination or precipitation) is supposed to obey a reaction-rate equation of type:

$$\frac{dc}{dt} = -kc^2 \tag{11}$$

where c is the spatial concentration of the involved defects or defect/antidefect pairs, and k is a characteristic time related to the mobility of the faster defect, and expressed as $k = KD_0e^{-\frac{H}{RT}}$, where H is the diffusion activation enthalpy.

Despite this drastic approximation, it can be shown that the parabolic Eq. (8) does reasonably represent not only defect recombination reactions, but also precipitation rates when, as in our case, these are strongly controlled by nucleation processes.

During a DSC measurement, temperature is a linear function of time (the heating rate is constant): $T = T_0 + At$, where A is the heating rate and T_0 the initial temperature. The expression of $c(t)$ is given by:

$$c(t) = \frac{AC_0e^{\frac{H}{T_0}+\frac{H}{At+T_0}}}{C_0D_0Ke^{\frac{H}{T_0}}(T_0+At) - e^{\frac{H}{T_0+At}}(Ae^{\frac{H}{T_0}} - C_0D_0KT_0) + C_0D_0HKe^{\frac{H}{T_0}+\frac{H}{T_0+At}}\left(E_i\left(\frac{H}{T_0+At}\right) - E_i\left(-\frac{H}{T_0}\right)\right)} \tag{12}$$

where C_0 is the initial value of c.

If a constant energy E_i is assigned to the annealing of defect i and M types of defects participate in the annealing process, the expression $\sum_i^M \frac{d}{dT}E_ic_i(T[t])$ provides a sufficiently accurate fitting function to attempt a peak analysis of the experimental curve $C_p^* = C_p^*(T)$ converted into energy release.

The total concentrations of defects in UO_2-10 estimated from different sources are reported in Table 1, for a storage time of 6 months. The calorimetric analysis shows that four peaks, corresponding to different defect annealing stages, are obtained (Fig. 13). All fitted parameters are reported in Table 2, which specifies the distinct physical significance of the various calorimetric stages. In the first row of Table 1, corresponding to oxygen Frenkel pairs, the upper limit is given (7.0×10^{21} cm^{-3}), as predicted by the cascade displacements (TRIM code, [3]) without recombination. The effective average concentration of 3×10^{20} cm^{-3} deduced from the lattice parameter change is the most accurate when compared to the results of the calorimetric analysis. However, this does not reveal which fraction of these defects was involved in the individual recovery stages, and how many defects were partially annealed in the metastable RT configurations observed by TEM (Fig. 2), which are likely responsible for the complex dependence of the lattice parameter increase as a function of defect concentration. Though the balance of the defect concentrations is affected by an uncertainty of the order of up to 20–30%, the analysis can be carried out by considering the features of the four recovery stages as follows.

Table 1
Defect concentrations (cm^{-3}) in UO_2-10 after α-damage accumulation during 6 months at room temperature α-Helium Inventory: 4.4×10^{18} atoms cm^{-3}.

Frenkel pairs	Oxygen	Uranium
From α-decay, with *no* account for multiple displacements (TRIM calculation)	7.0×10^{21}	1.9×10^{21}
From lattice parameter $a = f$(O/M)	3×10^{20}	3×10^{20}
From thermal diffusivity measurements	4×10^{20}	–

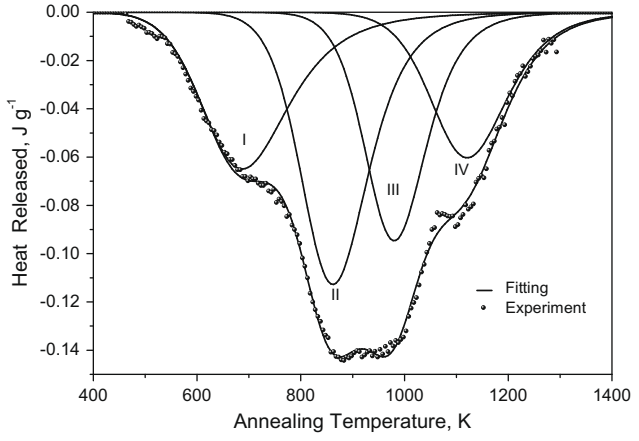

Fig. 13. Separation in four processes of the heat release observed during the DSC measurement for sample UO_2-10.

I. *Oxygen vacancy/interstitial recombination*: Since the oxygen Frenkel pair formation energy in UO_2 is sufficiently well known (3.8 ± 0.5 eV [17]), a defect concentration of 2.4×10^{20} cm^{-3} is deduced from the integral energy release. This implies that approximately 80% of defects created recombine during this stage. The resulting diffusion activation energy for oxygen recombination is 0.64 eV, *i.e.*, about one half of the diffusion energy of excess oxygen in UO_{2+x} [19].

II. *Uranium vacancy/interstitial clusters recombination*: The evaluation of the recombination energy can only be based on the hypothesis that the concentration of uranium vacancies is the same as that of oxygen. The argument in favour of this assumption is given by the preceding discussion of the lattice parameter annealing. An energy of 5.1 eV is found.

III. *Dislocation loop growth*: The following stages involve defects which escape recombination. Their fate in the given context is to precipitate to form loops or voids. The first are predominantly formed by interstitials and the second by vacancies. In both cases the oxide stoichiometry must be preserved, so that Schottky trios are needed to form lattice extra-planes or voids. Since the total length of the dislocation loops can be estimated from TEM micrographs at the end of this annealing stage, the concentration of defect involved can be deduced. The energy released by a Schottky trio captured by a dislocation loop results to be 10.6 eV.

IV. *Void growth*: In this last stage UO_2 vacancy complexes precipitate into voids, whose appearance is revealed by transmission electron microscopy. Here the concentration of defect can be easier measured as it corresponds to a first approximation to the void fractional volume, whose measured magnitude is of the order of 0.3 ± 0.05%. It is worthwhile noting that the corresponding vacancy trio's concentration is, within the experimental uncertainty, the same as the concentration of molecules forming loop extra-planes. The resulting defect annealing energy of a vacancy trio is 13.4 eV. The helium released during stage IV is very likely a consequence of the defect restructuring. In fact this takes place by short range migration of defects, while helium release entails migration distances of several orders of magnitude larger. It is however interesting that the measured activation energy for helium diffusion is the same as that of the activation for defect precipitation (2 eV).

Table 2
Defect concentrations and enthalpies in the four recovery stages deduced by DSC for the UO_2-10 sample after 6 months of damage accumulation.

Stage	I	II	III	IV
Total released energy	14.7 J g^{-1}	19.6 J g^{-1}	11.8 J g^{-1}	15.0 J g^{-1}
Mechanism	O vacancy–interstitial recombination	U vacancy–interstitial recombination	Loop formation	Void precipitation
Defects involved in recombination	2.4×10^{20} cm^{-3}		–	–
Defects involved in precipitation	–	–	7.0×10^{19} cm^{-3}	
Diffusion enthalpy, H	0.62 eV	1.34 eV	2.0 eV	2.0 eV
Reaction constant, K	1.4×10^{-18} cm^3 s^{-1}	3.7×10^{-15} cm^3 s^{-1}	2.1×10^{-13} cm^3 s^{-1}	1.9×10^{-12} cm^3 s^{-1}
Recovered energy, E	3.8 ± 0.5 eV	5.1 eV	10.6 eV	13.4 eV

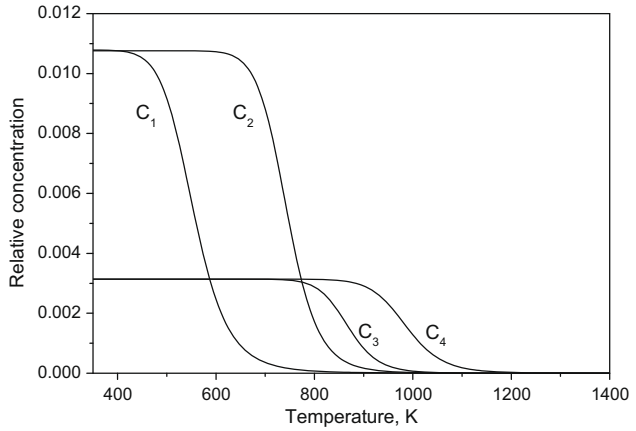

Fig. 14. Relative concentrations of the different kinds of irradiation defects during an annealing with heating speed of 0.5 K min^{-1}, similar to the one used during the thermal diffusivity measurements.

5.2. Evolution of the thermal conductivity during annealing

The evolution of the thermal conductivity during annealing depends on the concentration of the different kinds of point defects. These concentrations can be predicted for an annealing experiment of any heating speed using the model deduced from the interpretation of the DSC results (Eq. (12)). The relative concentrations C_i of the different kinds of defects ($c_i/2.23 \times 10^{22}$, where 2.23×10^{22} is the number of UO_2 per cm^3) are plotted in Fig. 14 for an annealing speed similar to the one used during the thermal diffusivity measurements (0.5 K min^{-1}).

The annealing experiments for the UO_2-10 sample can be used to determine the parameters required to describe the temperature dependence of the recovery. The measured decrease for the A coefficient (Fig. 9) is $\Delta A_1 = 0.13$ mK W^{-1} for the first step and $\Delta A_2 = 0.07$ mK W^{-1} for the second step. A small supplementary decrease of about 0.02 mK W^{-1} is observed in the temperature range 1000–1200 K. To a first approximation, this small recovery is attributed to stages three and four with an amplitude of $\Delta A_3 = \Delta A_4 = 0.01$ mK W^{-1}. The total variation of the A coefficient is of 0.22 mK W^{-1} consistently with the value of obtained using Eq (8).

The relative concentration of defects corresponding to the saturation of thermal conductivity degradation, C_{iS}, can be approximated by comparing the annealing behaviour of the defects concentrations and the simultaneous recovery of the thermal diffusivity during the annealing experiment. For instance, the first step of thermal diffusivity recovery is observed at ~600 K (Fig. 9), while at that moment $C_{1S} \approx 0.0025$ (Fig. 14). This means that, because of the saturation effect, the thermal conductivity begins to recover only after C_1 has decreased by about 75%. A similar value $C_{2S} \approx 0.0025$ is found for the second stage, and $C_{3S} \approx C_{4S} \approx 0.0005$ for the third and fourth stages. For the first recovery step, the concentration C_1 decreases while temperature increases, but no recovery effect on the thermal conductivity is observed until C_1 is equal or lower as C_{1S}. When $C_1 < C_{1S}$, it is supposed that the thermal conductivity recovery is proportional to C_1 and the decrease of the A coefficient is given by $A_1\, C_1/C_{1S}$. If the same approach is used for the four annealing steps, the resulting evolution of the A and B coefficients during annealing is in good agreement with the experiment (Fig. 15).

Schmidt et al. [16] evaluated the relative concentration of defects corresponding to the saturation of thermal conductivity

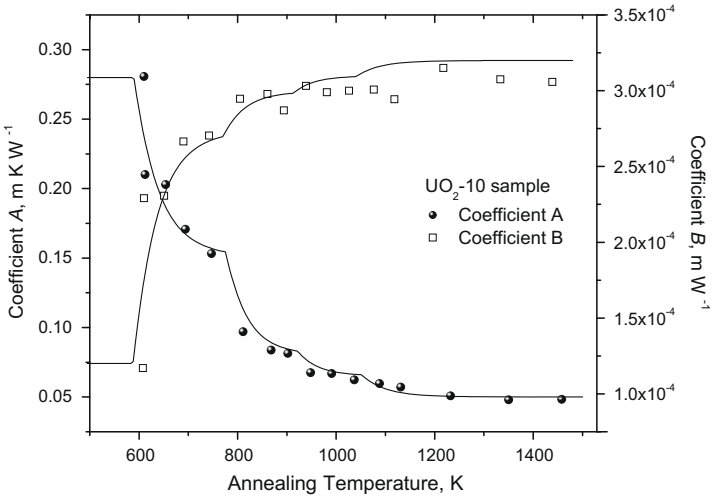

Fig. 15. Measured and modelled variation during annealing of the A and B coefficients of the thermal conductivity. The model assumes an annealing behaviour with steps as obtained from the interpretation of the DSC measurement.

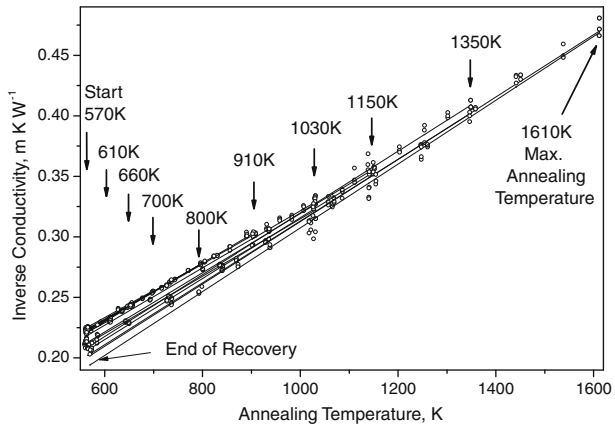

Fig. 16. Inverse thermal conductivity of the UO_2 VOLEX sample (nine subsequent annealing cycles) irradiated to 0.4 MWd/t at a constant temperature of 570 K.

degradation to be $\approx 4 \times 10^{-3}$. This value is of the same order of magnitude as the total concentration that results from the contribution of the different kinds of defects as evaluated in this work (6×10^{-3}).

6. Thermal diffusivity recovery of reactor-irradiated samples

The thermal diffusivity of the VOLEX samples irradiated to about 0.4 MWd/t at 570 K was measured by the laser-flash technique. The measurements have been performed by 10 subsequent thermal annealing cycles with a constantly increasing maximum temperature in the range from 570 K to 1600 K (Fig. 16). Three main recovery stages were observed at nearly the same temperatures, as previously found for high burn-up fuels [1], namely at approximately 650 K, 1000 K and 1300 K.

The thermal conductivity was obtained from the thermal diffusivity and then interpolated by the function $1/(A + BT)$. Fig. 17 shows the dependence of A and B on the annealing temperature. The temperatures corresponding to the recovery stages are in agreement with the results obtained for the α-doped samples. This shows that fission and α decay produce defects having the same nature and annealing behaviour and confirms the relevance of the studies performed on α-damaged samples.

7. Summary and conclusions

Experiments were performed on α-doped and reactor-irradiated samples with the aim to obtain a precise description of radiation damage and of its effect on the thermal conductivity. The results indicate that the damage effects and the recovery phenomena during thermal annealing occur by similar mechanisms both in α- and fission-damaged UO_2. The description of the radiation damage nature (point defects, dislocations, voids) and concentration can not be achieved with a single experiment. It requires the combination of direct observation (TEM, SEM for dislocations and voids) with measurements of thermophysical properties sensitive to its concentration. In this work, lattice parameter, apparent specific heat and thermal diffusivity were measured during annealing experiments. Furthermore, the release of the helium created in the alpha doped samples was investigated by Knudsen-cell mass spectrometry in order to clarify its role in the recovery mechanisms. Finally, information form the literature was also used, in particular for the identification of the point defects nature and migration or recombination energies.

The thermal diffusivity is very sensitive to the concentration of defects and its thermal recovery can be used to determine the temperature ranges where healing of the different kinds of defects takes place. Thermal diffusivity degradation does not depend linearly on the concentration of defects and therefore it is not best suited to estimate their effective concentration and properties. Also, this measurement is not continuous as a function of temperature because the recovery is measured using a limited number of thermal annealing cycles.

Calorimetric measurements show that annealing of defects produces measurable heat. This measurement is well adapted to the analysis of radiation damage recovery because it is continuous as a function of temperature and uses a constant heating rate. Four distinct annealing stages were observed whose identification was made possible by a comparative analysis with the independent recovery processes of lattice parameter, thermal diffusivity, void/dislocation growth and α-helium release. The first two stages are attributed to recombination of O- and U- defects, respectively. These point defects are the main cause of the thermal diffusivity degradation. From empirical estimates of the concentrations of defects present in the examined samples, their energies of recombination were deduced. In particular, the value for uranium probably represents the most accurate *direct* measurement obtained so far.

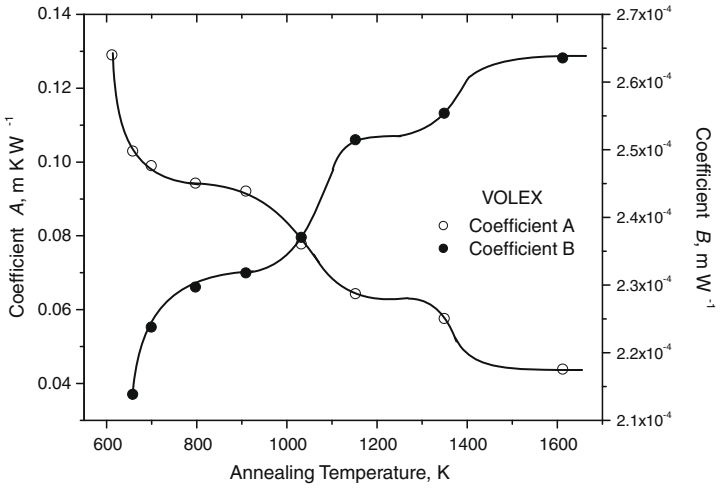

Fig. 17. A and B coefficients of the $1/(A + BT)$ law interpolating the thermal conductivity, as a function of the maximum annealing temperature for the VOLEX (UO_2) sample. Lines are a guide for the eye.

After the two stages during which complementary defect annihilate, loops and void precipitation give rise to two subsequent energy release stages. In both cases co-precipitation of oxygen and uranium defects is needed. The diffusion enthalpies of these stages are clearly higher than in the first two stages during which single defect atomic jumps were involved, indicating that mobile defect clusters are formed. The energies released in forming interstitial loops and voids are compatible with the expected concentration of Schottky trios formed by defects surviving recombination.

Precipitation of helium in-solid does not produce visible calorimetric effects. The diffusion and release of gas takes place at the end of stage IV, when dislocations are well developed and voids are formed. An interesting observed feature is that helium is scarcely trapped by voids, so that its diffusion is not strictly associated to that of vacancies.

A correlation for the effect of the different kinds of radiation defects on the thermal conductivity was obtained by combining the results of the calorimetric and thermal diffusivity measurements. This result is also useful in order to provide information on the evolution of the state of spent fuel under final or interim storage conditions. A practical application of this result is that the thermal conductivity degradation of stored spent-fuel can be expected to level off after a few years of storage.

The results obtained for very low burn-up fuel using the VOLEX reactor-irradiated sample have shown that the build-up of fission damage and its effect on the thermal conductivity is appreciable already at very low burn-ups, and that the annealing behaviour is similar to the one observed in auto-irradiated samples.

Acknowledgments

The authors would like to thank G. Pagliosa, M. Jörgensen, M. Sheindlin, J. Cobos and P. Boulet for their participation in the experimental work. We gratefully acknowledge J. Somers, C. Fuchs and D. Papaioannou for the preparation of the samples.

References

[1] C. Ronchi, M. Sheindlin, D. Staicu, M. Kinoshita, J. Nucl. Mater. 327 (2004) 58.
[2] V.V. Rondinella, H.J. Matzke, J. Cobos, T. Wiss, Mater. Res. Soc. Symp. Proc. 556 (1999) 447–454.
[3] J.F. Ziegler, J.P. Biersack, U. Littmark, The Stopping and Range of Ions in Solids, Pergamon Press, Oxford, 1985.
[4] T. Ohmichi, S. Fukushima, A. Maeda, H. Watanabe, J. Nucl. Mater. 102 (1981) 40–46.
[5] S. Fukushima, T. Ohmichi, A. Maeda, M. Hanada, J. Nucl. Mater. 114 (1983) 260–266.
[6] C. Duriez, J.P. Alessandri, T. Gervais, Y. Philipponneau, J. Nucl. Mater. 277 (2000) 143.
[7] M. Amaya, T. Kubo, J. Nucl. Sci. Technol. 33 (8) (1996) 636–640.
[8] W.J. Weber, J. Nucl. Mater. 114 (1983) 213–221.
[9] W.J. Weber, Radiat. Eff. 83 (1984) 145–156.
[10] A.O.R. Cavaleru, C.M. Morley, D.G. Armour, G. Carter, Radiat. Eff. 18 (1973) 87.
[11] R. Evron, G. Kimmel, Y. Eyal, J. Nucl. Mater. 217 (1994) 54–66.
[12] N. Nakae, A. Harada, T. Kirihara, J. Nucl. Mater. 71 (1978) 314–319.
[13] M. Sheindlin, D. Halton, M. Musella, C. Ronchi, Rev. Sci. Instrum. 69 (3) (1998) 1426.
[14] W. Wiesenack, in: Proceedings of the ANS International Topical Meeting on LWR Fuel Performance, Portland, Oregon, USA, March 2–6, 1997.
[15] J.J. Carbajo, G.L. Yoder, S.G. Popov, V.K. Ivanov, J. Nucl. Mater. 299 (2001) 181–198.
[16] H.E. Schmidt, J. Richter, H.-J. Matzke, J.V. Geel, in: T. Tong (Ed.), Thermal Conductivity, vol. 22, Technomic Pub. Co., Inc., 1999.
[17] H.J. Matzke, J. Chem. Soc. Faraday Trans. 83 (1987) 1121–1141.
[18] A.D. Brailsfrod, R. Bullough, Physical Metallurgy of Reactor Fuel Elements, The Metals Society, 1975.
[19] A.B. Auskern, J. Bell, J. Nucl. Mater. 3 (1961) 267.
[20] V.V. Rondinella, T. Wiss, J.P. Hiernaut, in: Proceedings of the ICEM '03, Oxford, UK, September 21–25, 2003, ASME 2003 (CD-ROM).
[21] C. Ronchi, J.P. Hiernaut, J. Nucl. Mater. 325 (1) (2004) 1–12.